2D/3D Perovskite Engineering Eliminates Interfacial Recombination Losses in Hybrid Perovskite Solar Cells

Albertus Adrian Sutanto
EPFL https://orcid.org/0000-0002-9413-2789
Pietro Caprioglio
University of Potsdam https://orcid.org/0000-0002-3465-2475
Nikita Drigo
EPFL
Yvonne Hofstetter
TU Dresden
Ines Garcia Benito
EPFL
Valentin Queloz
École Polytechnique Fédérale de Lausanne
Dieter Neher
University of Potsdam https://orcid.org/0000-0001-6618-8403
MOHAMMAD KHAJA Nazeeruddin
École Polytechnique Fédérale de Lausanne https://orcid.org/0000-0001-5955-4786
Martin Stolterfoht
University of Potsdam https://orcid.org/0000-0002-4023-2178
Yana Vaynzof
TU Dresden https://orcid.org/0000-0002-0783-0707
Giulia Grancini (✉ giulia.grancini@unipv.it)
University of Pavia https://orcid.org/0000-0001-8704-4222

Article

Keywords: 2D engineering, 3D engineering, device interface, solar cells

Posted Date: August 12th, 2020

DOI: https://doi.org/10.21203/rs.3.rs-51900/v1

Version of Record: A version of this preprint was published at Chem on July 1st, 2021. See the published version at https://doi.org/10.1016/j.chempr.2021.04.002.

2D/3D Perovskite Engineering Eliminates Interfacial Recombination Losses in Hybrid Perovskite Solar Cells

Albertus A. Sutanto[1], Pietro Caprioglio[2,3], Nikita Drigo[1], Yvonne J. Hofstetter[4], Ines Garcia-Benito[1], Valentin I. E. Queloz[1], Dieter Neher[2], Mohammad Khaja Nazeeruddin[1]*, Martin Stolterfoht[2]*, Yana Vaynzof[4,]*, Giulia Grancini[1,5]*

[1]Group for Molecular Engineering of Functional Materials, Institute of Chemical Sciences and Engineering, EPFL Valais Wallis, Rue de l'Industrie 17, CH-1951 Sion, Switzerland.

[2] University of Potsdam, Institut für Physik und Astronomie, Potsdam, Germany

[3] Young Investigator Group Perovskite Tandem Solar Cells, Helmholtz-Zentrum Berlin für Materialien und Energie GmbH, 12489 Berlin, Germany

[4] Dresden Integrated Center for Applied Physics and Photonic Materials (IAPP) und Centre for Advancing Electronics Dresden (cfaed), Technical University of Dresden, 01062 Dresden

[5] Department of Chemistry and INSTM, University of Pavia, Via T. Taramelli 14, 27100 Pavia, Italy.

* email: giulia.grancini@unipv.it, yana.vaynzof@tu-dresden.de, stolterf@uni-potsdam.de, mdkhaja.nazeeruddin@epfl.ch

Engineering two-dimensional (2D) / three-dimensional (3D) perovskites has emerged as an attractive route to efficient and durable perovskite solar cells. Beyond improving the surface stability of the 3D layer and acting as a trap passivation agent, the exact function of 2D/3D device interface remains

vague. Here, we provide evidence that 2D/3D perovskite interface that forms a *p-n* junction is capable to reduce the electron density at the hole-transporting layer interface and ultimately suppress interfacial recombination. By a novel ultraviolet photoelectron spectroscopy (UPS) depth-profiling technique, we show that engineering of the 2D organic cations, in this case by simply varying the halide counter ions in thiophene methylammonium-salts, modifies the 2D/3D perovskite energy alignment. These measurements enable the true identification of the energetic across the 2D/3D interface, so far unclear. When integrated in solar cells, due to the electron blocking nature of the 2D layer, the optimized 2D/3D structures suppress the interfacial recombination losses, leading to open-circuit voltage (V_{OC}) which approaches the potential internal Quasi-Fermi Level Splitting (QFLS) voltage of the perovskite absorber. The devices exhibit an improved fill factor (FF) driven by the enhanced hole extraction efficiency and reduced electron density at the 2D/3D interface. We thus identify the essential parameters and energetic alignment scenario required for 2D/3D perovskite systems in order to surpass the current limitations of hybrid perovskite solar cell performances.

Understanding and exploiting interfacial physics is key in perovskite solar cell engineering and optimization.[1,2] That is especially true when interface losses play a dominant role and complex interface functionalization is essential to minimize them. In the field of hybrid perovskite engineering, much attention has been lately focused on multi-dimensional perovskite interfaces consisting of a wider band gap layered (namely, two dimensional-2D) perovskite deposited between the bulk 3D perovskite and the hole transporting layer (HTL) in a standard mesoporous configuration.[3-9] Such configuration is currently among the most effective strategies to enhance both the efficiency and stability of perovskite solar cells.[3,10,11] It is generally considered that the 2D perovskite acts as both an efficient mean to passivate the surface traps (leading to reduced defect recombination) and an electron blocking layer due to its wider band gap.[12-15] However, despite these empirical observations, the energetic alignment at the interface and the relative function of the 2D/3D interface is only qualitatively depicted with a only a partial understanding of these

aspects. This lack of knowledge prevents the advancement of device efficiencies towards the theoretical Shockley-Queisser predictions beyond the common trial and error approach.[16] More specifically, the exact role of the interface band structure and energetics and their effect on the processes and loss mechanisms remains largely unexplored, mainly due to the lack of direct experimental evidences. In this work we target the interface energetics of optimized 2D/3D perovskite systems by measuring the vertical energy level landscape by an innovative UPS depth profiling technique. The analysis reveals intriguing variations of the interfacial energetics which depend on the chemical nature of 2D overlayer. Specifically, we explore a series of thiophene based cations that form the 2D perovskite layer, which differ slightly in their chemical structure, and which when integrated in a 2D/3D based perovskite solar cell, deliver approximately 21% power conversion efficiency and open-circuit voltage (V_{OC}) approaching 1.2 V. The photovoltaic performance is intimately linked to 2D/3D interfacial band bending and a natural formation of a *p-n* junction in optimal devices. By calculating the quasi-Fermi level splitting (QFLS) from photoluminescence quantum yield (PLQY) for the neat material and the complete device, we identify that the optimal energetic alignment and reduced electron density at the interface serve as the reasons for such a drastic reduction in the non-radiative interfacial recombination losses. Notably, the optimal material exhibits an extremely high PLQY of 5-6%, far beyond the best values reported in literature of around 1 %[17,18] and, in the device, the PLQY approaches 2% which is far above average.[2] Importantly, the recombination mechanisms proposed is corroborated by drift-diffusion simulation. The optimized 2D/3D interface reaches the QFLS-potential of the neat perovskite absorber and nullifies the energy losses at the interfaces. As such, we rationalized the mechanisms and the effect of 2D/3D interfaces on the effective reduction of the interfacial energy losses, providing a clear path for pushing perovskite solar cells performances closer to their theoretical limits.[2]

The 2D/3D interfaces investigated here are based on a novel set of bulky thiophene-terminated cations, namely 2-thiophenemethylammonium iodide (2-TMAI),[9,19] 2-thiophenemethylammonium bromide (2-TMABr), and 2-thiophenemethylammonium chloride (2-TMACl) that serve as a building block for the formation of the 2D perovskite layer on top of 3D bulk layer (Fig. 1a). The 3D perovskite layer is based on

a triple-cation composition $[(FAPbI_3)_{0.87}(MAPbBr_3)_{0.13}]_{0.92}(CsPbI_3)_{0.08}$ with a bandgap of 1.610 eV. The chemical structures of the thiophene-methylammonium salts are shown in

Fig. **1**b. The three different 2-thiophenemethylammonium halides (2-TMAX, where X: Cl, Br, I) were prepared from the commercially available amines and the corresponding acids (see experimental methods). The salts were then diluted in isopropanol (IPA) and dynamically spin-coated on top of the triple-cation based 3D perovskite film. 2D perovskites are selectively grown by controlling the excess PbI_2 composition (PbI_2:FAI = 1.05:1) in the 3D perovskite which reacts with the thiophene ammonium halide cations to form the 2D layer.[4,9,19] Fig. 1b shows also the X-ray diffraction (XRD) patterns of the 2D/3D films collected at a low diffraction angle. When the 2-TMAX is used to coat the 3D layer, intense reflexes at 4.3° and 8.6° appear at the XRD diffractograms, consistent with the key characteristic peaks of 2D perovskites.[9,19] The XRD pattern of 3D perovskite layer as the control are reported on Supplementary Fig. 1. Cross-sectional scanning electron microscopy (SEM) images shown in Fig. 1c show that the 500 nm thick 3D perovskite layer is continuously coated by a 2D overlayer with a thickness of approximately 50 nm. The top surface images reveal that the formation of the 2D layers results in smoother surfaces, with less defined grain boundaries and crystals borders. This is particularly evident for the cases of 2-TMAI and 2-TMABr, while

for the case of 2-TMACl a distribution of distinct phases with larger and more elongated grains is visible.

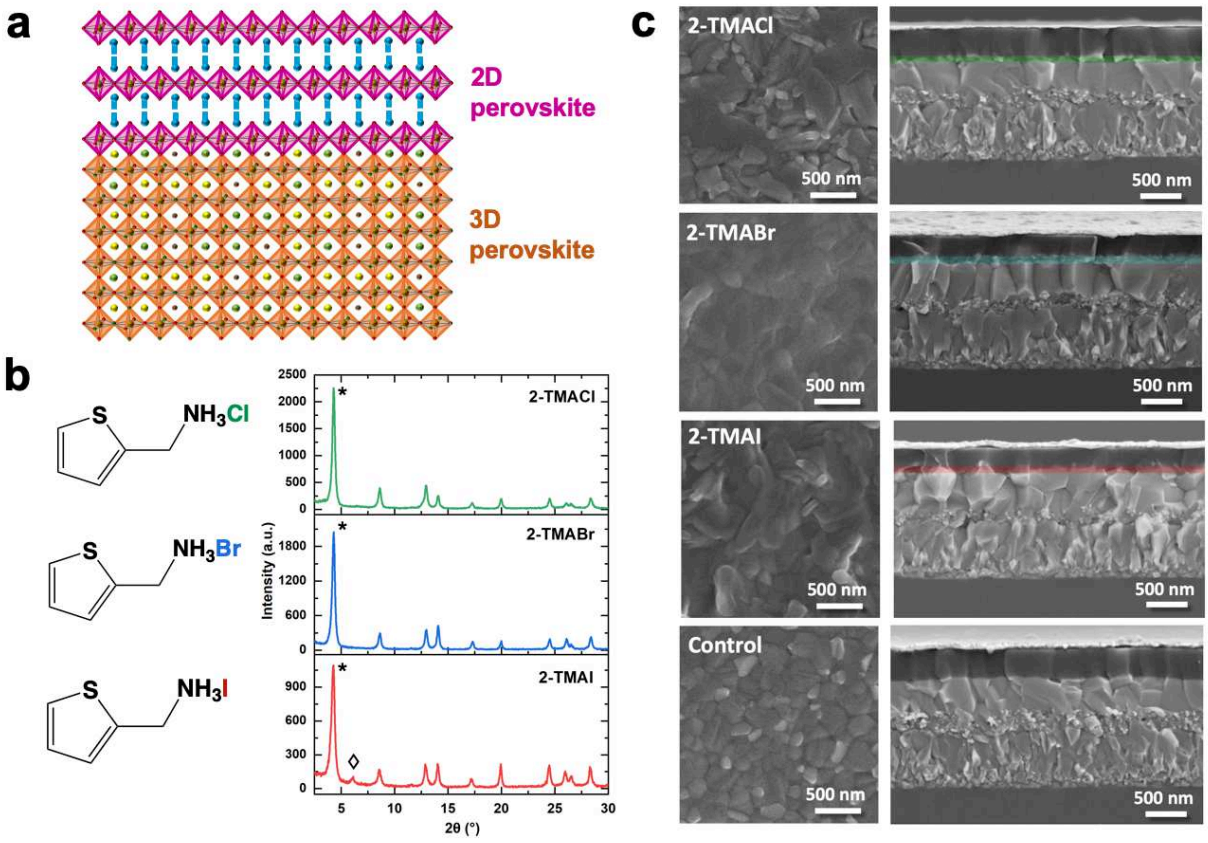

Fig. 1 Structural and morphological characterization of 2D/3D perovskite films. a Schematic illustration of the 2D/3D perovskite interface. **b** Molecular structure (left) and X-ray diffraction (XRD) pattern at 2° incident angle of the 2D/3D film employing 2-TMAI, 2-TMABr, and 2-TMACl respectively (* and ◊ denote 2D perovskite phase with n=1 and n=2, respectively). **c** Top view (left) and cross-section (right) micrographs of the 3D only device as control and the 2D/3D perovskite solar cells (PSCs) employing 2-TMAI, 2-TMABr, and 2-TMACl.

The absorption spectra of the 2D/3D thin films are reported in Supplementary Fig. 2, while Supplementary Fig. 3 shows the PL spectra upon excitation from the front side of the film. Notably, in all cases, a clear peak at lower wavelength region is observed, confirming to the formation of a distinct 2D perovskite overlayer. More in details, in agreement with what we recently reported,[9] the 2-TMAI-based 2D/3D shows a slightly reduced band gap with respect to the 2-TMABr and 2-TMACl, as revealed by the photoluminescence peak emission shift (of around 0.1eV) in Supplementary Fig. 3.

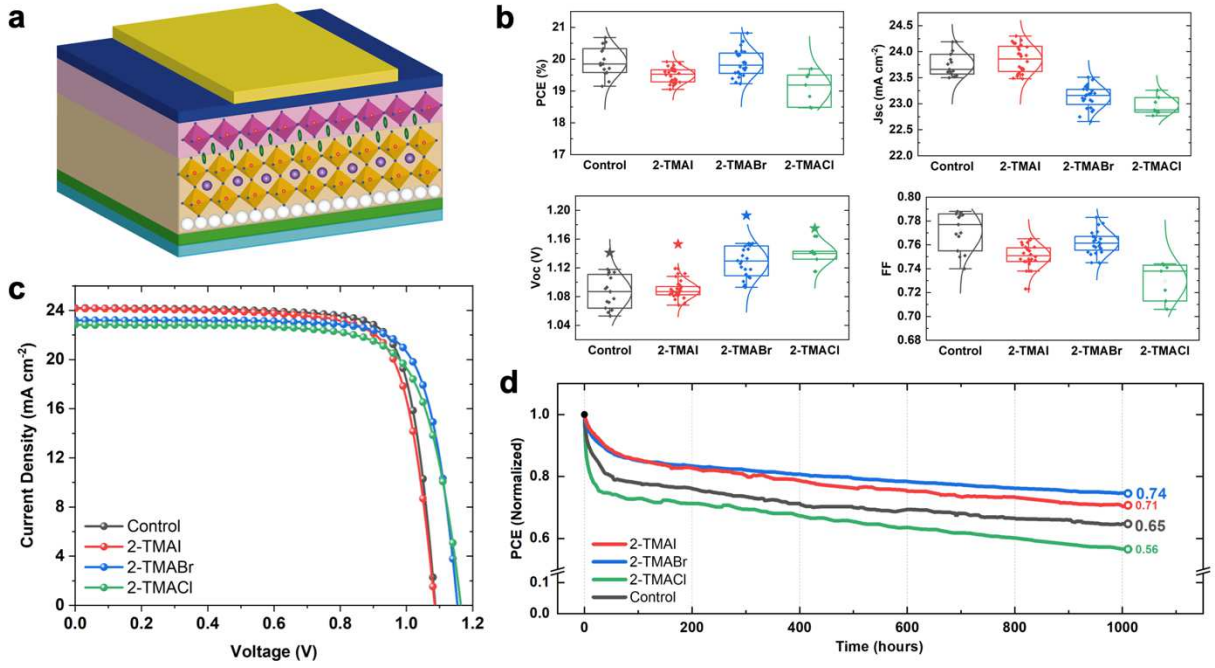

Fig. 2 Photovoltaic performances of 2D/3D perovskite solar cells (PSCs). **a** Schematic device structure of the 2D/3D PSCs. **b** Statistics of the photovoltaics parameters of 3D PSCs as a control and 2D/3D PSCs based on 2-TMAI, 2-TMABr, 2-TMACl on over 70 devices. Note that the stars symbols in the V_{OC} subpanel represent the V_{OC} measured without using a mask. **c** *J-V* curves of the champion cells of 3D and 2D/3D PSCs employing 2-TMAI, 2-TMABr, and 2-TMACl. **d** Stability test under continuous 1 sun illumination for 1000 h in inert gas (Ar) atmosphere without any encapsulation.

The photovoltaic (PV) response of the 2-TMAX based 2D/3D perovskite solar cells are shown in Fig. 2 with the PV parameters for champion devices summarized in Table 1. With respect to the control, a clear increase in the V_{OC} is observed with the 2D perovskite layer, higher for 2-TMABr and 2-TMACl. It is important to note that the device V_{OC} reported here is underestimated due to the use of a small mask (0.16 cm^2) on a large pixel (0.54 cm^2). Considering that the dark current of the pixel is not affected by the mask, this implies a ~3.4-fold overestimation of the dark saturation current (J_0), which is equivalent to a voltage loss of 31 mV. By measuring without mask, the real maximum device voltage (shown by stars in Fig. 2b) for the reference cell is 1.141 V, while for 2-TMAI, 2-TMABr and 2-TMACl, they are 1.153 V, 1.193V and 1.175V, respectively (see also Supplementary Fig. 4), among the highest values reported so far for *n-i-p* devices with a mesoporous structure.

Importantly, the 2-TMABr shows a remarkable increase in V_{OC}, without compromising the fill factor (FF) which remains comparable to the control device, resulting in an overall increase in the device efficiency. On the other side, the 2-TMACl shows a reduction of the FF. The highest PV performance is therefore achieved with 2-TMABr-based 2D devices delivering a power conversion efficiency (PCE) of 20.82%. We note that this series of 2D perovskites, a slight decrease in the short-circuit current (J_{SC}) is observed. This decrease might be related to the limitation in the charge transport induced by the presence of the bulky organic moieties. The long-term stability of the devices was monitored under continuous illumination of 1-sun intensity for 1000 hours in an argon atmosphere and is shown in Fig. 2d. While the performance of the standard 3D device is reduced to 65% of its initial PCE, the 2D-functionalized solar cells shows a reduced loss in the PCE with the 2-TMABr/3D devices displaying the best stability retaining 75% of the initial PCE after 1000 hours. This confirms that the 2D surface functionalization has a crucial impact on the device lifetime with best performances reached with the 2-TMABr based 2D perovskite. 2D/3D perovskite devices are demonstrated to be highly sensitive to the nature of the organic cation which impact on the device V_{OC} and FF.

To elucidate the link between material properties and device performances, it is necessary to directly probe the energetic alignment of the 2D/3D interfaces. Traditional methodology based on UPS measurements is only capable of probing the top 1-2 nm of the surface and will not provide insights regarding the buried 2D/3D interface. Recently, we developed a novel method termed ultra-violet photoemission spectroscopy (UPS) depth profiling technique, which allows probing the energetic landscape at the bulk of materials and across buried interfaces.[20] The principle of the technique is shown in Fig. 3a and is based on the essentially damage-free etching enabled by Argon gas-cluster ion beams (1) in combination with UPS measurements (2) after each etching step. This method allows the accurate measurement of the progression of the vacuum level and valence band positions as a function of film depth (Fig. 3b), providing for the first time an in-situ measurement of the interfacial energy levels alignment (Fig. 3c). The position of the conduction band is then estimated by adding the corresponding optical gap. The method has already been applied to a range of organic and organic/inorganic systems,[21-23] and here we apply it for the first time to study the interfacial alignment of 2D/3D perovskites.

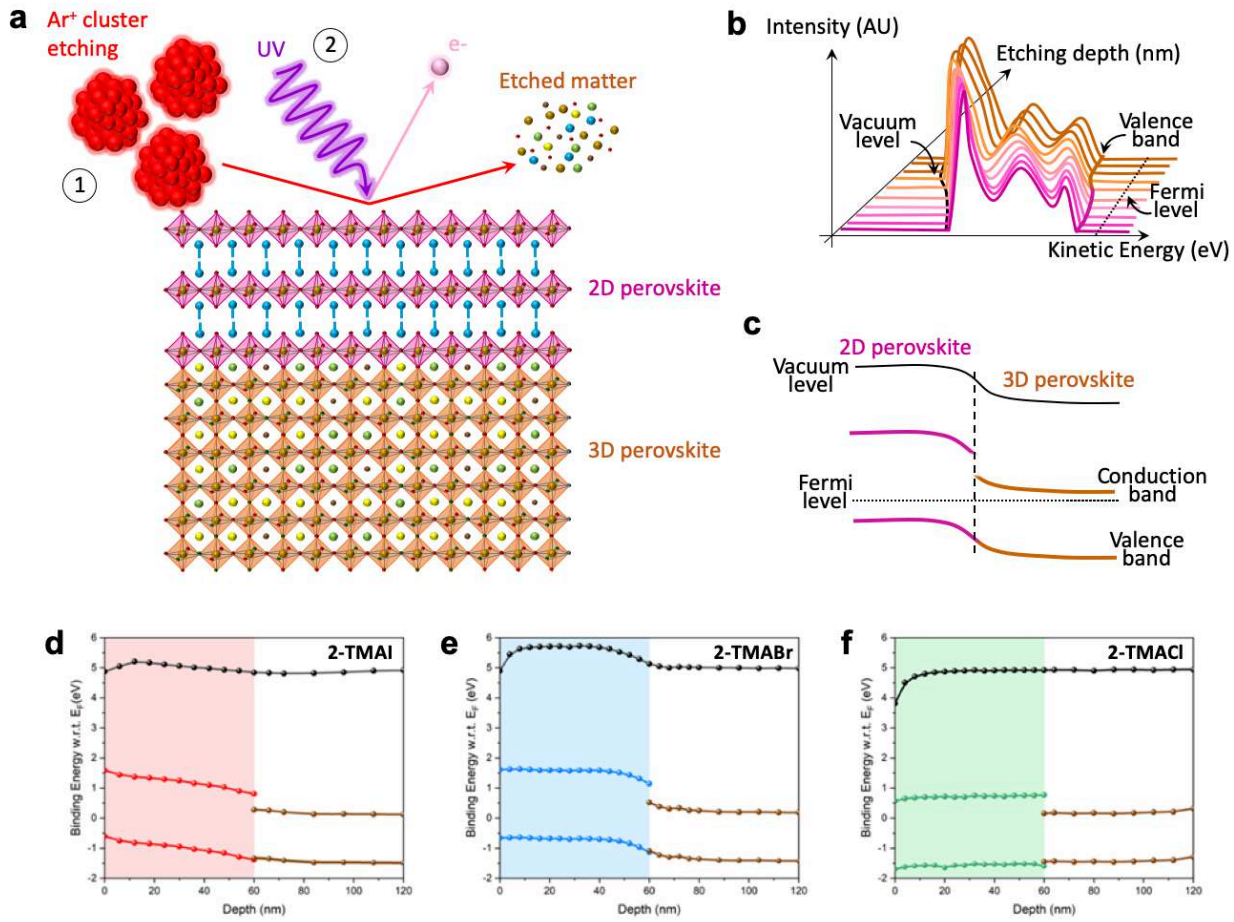

Fig. 3. UPS depth measurement of 2D/3D perovskite interface. a Schematic representation of the UPS depth profiling technique which combines (1) etching by Ar ion clusters with (2) UPS measurements. **b,c** illustration of the evolution of the UPS spectra as a function of depth (**b**) and the corresponding energy level diagram extracted from **b** (**c**). **d-f** Measured energetic level diagrams of 2-TMAI **(d),** 2-TMABr **(e)**, and 2-TMACl **(f)** with the 3D perovskite layer.

UPS depth profiling of the three sets of 2D/3D samples reveals significant differences in their interfacial energetic alignment. Examining the band structure, it is clear that exchanging the halide on the bulky cations has important consequences for the evolution of the valence band levels: i) 2-TMABr and 2-TMAI show a shift in valence band compared to the 3D perovskite, indicating an effective energy level alignment to promote hole extraction, while 2-TMACl exhibited an opposite trend, with a slight uphill energy barrier (over the entire 2D layer). This results in the first two cases in the formation of a *p-n* junction which promotes charge extraction. Notably, this is consistent with the low FF observed in the 2-TMACl 2D/3D devices. ii) All the 2D/3D interfaces exhibit excellent electron blocking properties, with the energetic barrier being enhanced from 0.53 eV for 2-TMAI to 0.62 eV and 0.61eV for 2-TMABr and 2-TMACl, respectively. The improvement in electron blocking suggests a more efficient reduction of minority carriers at the HTL interface of the device, in good agreement with corresponding enhancement in the open-circuit voltage observed from the photovoltaic results. Notably, in all cases, the 3D perovskite is *n-type*, in agreement with the PbI_2 excess used in this case.[24] Surprisingly, while the 2D layer formed by the 2-TMACl cation follows a similar character to that of the 3D perovskite, 2-TMABr and 2-TMAI denote a clear transition toward a *p-type* material. Such a transition is responsible for the formation of a *p-n* junction at the interface offering the possibility to improve the charge extraction and reduce interface recombination. This is particularly evident for the 2-TMABr case as well as for the 2-TMAI case, while it is less manifested at the 2-TMACl based interface, possibly due to a less homogeneous 2D surface layer (see SEM top view in Fig. 1c). As such, this proves that band bending happens at optimized 2D/3D perovskite interface, contributing in improving the device performance, as reported for other PV technologies.[25]

These results are also supported by numerical drift-diffusion device simulations, based on a well-established model,[26-31] which compare the effect of the additional 2D layer and the different energetic alignment scenarios based on the experimental results obtained for the reference 3D sample, 2-TMABr and 2-TMACl (Supplementary Fig. 5a-c). The effect of the enhanced electron blocking at the 2D/3D interface is evident when comparing the carrier densities in the proximity of the HTL interface (Supplementary Fig.

5d-f, dashed red circle). In the case of 2D/3D systems, the electron density at that interface is significantly reduced when compared to the reference 3D case. In excellent agreement with the experimental J-V results, when incorporating the 2-TMABr layer into the device structure, the simulated V_{OC} increases from ~1.14V to ~1.19V (Supplementary Fig. 5g). This increase can be attributed to the strong reduction of the electron density in the 2D in the proximity to the HTL which effectively limits the interfacial recombination losses (see Fig. 3b).[32] Overall, in case of the 2-TMABr cation, the band bending reduces the electron accumulation at the interface with the HTL, thereby reducing charge recombination while effectively driving holes to the HTM without inducing FF losses. Together these processes provide an effective mean to eliminate the severe non-radiative recombination loss at the HTM/perovskite interface.

To further corroborate these findings and to understand the physical processes governing these 2D/3D interfaces triggering the improvement in device V_{OC}, we measured the photoluminescence quantum yield (PLQY) and derived the Quasi Fermi Level Splitting (QFLS) in neat materials and complete solar cell devices. This analysis allowed us to assess the relative contribution of bulk and interfacial recombination losses, but also the impact of the interfacial energy alignment.[2,29,33] First of all, it is important to remark that our optimized materials exhibit an extremely high PLQY of 5-6% (see Supplementary Fig. 6a,c), far beyond the best values reported in literature, usually of around 1%.[17,18] In addition, the device PLQY approaches 2% which is far above average (see Supplementary Fig. 6b,c).[2]

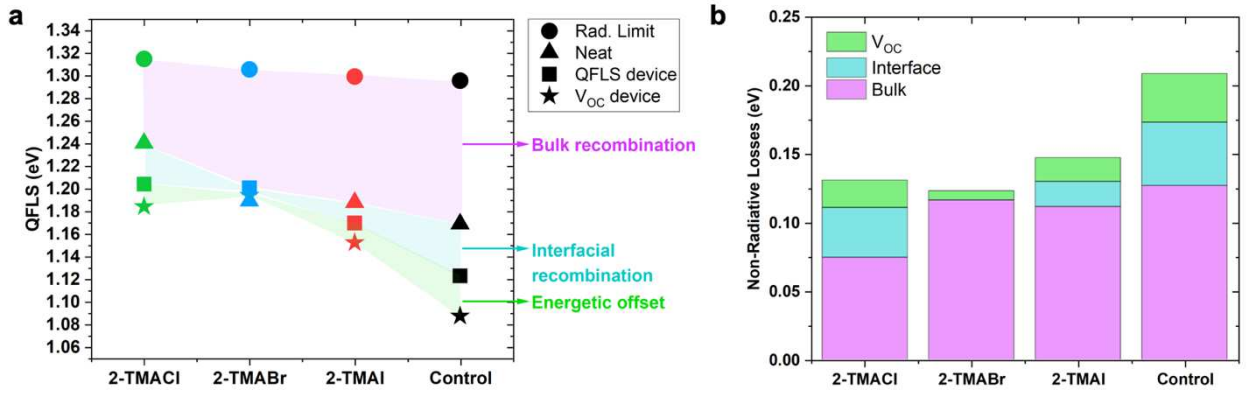

Fig. 4. Calculated QFLS and calculated energy losses due to non-radiative recombination. a QFLS calculated from PLQY for the neat material and the full device for the different samples investigated in the study. Here the Shockley-Queisser radiative limit and the experimental V_{OC} of each sample are plotted. **b** Different type of energy losses calculated from **a** in order to compare the contribution of the different recombination processes for each system.

The results highlight that the addition of a 2D layer already improves the QFLS of the neat perovskite absorber indicating trap passivating behavior and possibly the reduction of minority charges from the defect-dense perovskite. The overall trend in non-radiative losses follows the trend observed in the J-V measurements. Interestingly, when the QFLS of the device is compared to the neat material, we found that all devices that employ the 2D layer display minimal energy losses due to lower interfacial recombination losses compared to the reference cell. This confirms a key conclusion from the UPS measurements and the numerical simulations, which is that the 2D layer effectively reduces the density of minority carriers at the HTL interface. Notably, the device implementing 2-TMABr as cation exhibits an equal QFLS in the neat material and in the complete device, highlighting the presence of a lossless perovskite/HTL interface. Therefore, the 2D layer enables to reach the QFLS-potential of the neat perovskite layer.[2] These results are in accordance to the UPS depth profiling and simulations data. The formation of the *p-n* junction leads to a matching between the internal QFLS and V_{OC} in the device which is also consistent with perfect energetic alignment between the perovskite and the HTL.[28,29] Notably, in the case of the reference device, the internal QFLS is significantly higher than the external V_{OC}, suggesting an energy misalignment between the perovskite and the Spiro-OMeTAD which can promote interface recombination.[28] In 2D/3D systems, this effect is nullified due to electron blocking nature of the 2D overlayer and the formation of a *p-n* junction.

In conclusion, we demonstrate that even subtle changes in the composition of the 2D perovskite can lead to differences of the energetic alignment at the 2D/3D interface, with a direct impact on charge density distribution, interfacial recombination and ultimately device performance. Our results highlight that UPS

depth profiling is a valuable method that allows to directly probe the interfacial alignment and band bending, which is essential to drive interfacial chemistry and proper functionalization for a smart device optimization. Combining chemical manipulation of the 2D perovskite and deep understanding of the 2D/3D interface energetics and recombination processes, our results provide clear evidence that 2D/3D interface engineering with optimal energetics allows to nullify the non-radiative interfacial recombination of electron and holes, demonstrating a breakthrough in the path to further enhance perovskite solar cell performance.

Methods

Synthesis of thiophenemethylammonium halides

A concentrated aqueous solution of an acid HX (1.1 eq, where X:Cl, Br or I) was added drop by drop to 1.0 M ethanol solution of thiophenemethylamine (1.0 eq) at 0°C under stirring. The mixture was allowed to reach room temperature gradually and then it was poured into an excess of diethyl ether (Et_2O). The precipitate was separated and washed thoroughly with Et_2O. The salts were recrystallized from ethanol (EtOH) and Et_2O mixtures, resulting in crystalline solids of the salts.

Perovskite thin-film and solar cells devices fabrication

Fluorine-doped tin oxide (FTO) substrates (Nippon Sheet Glass) were patterned by chemical etching process using zinc powder and aqueous HCl solution (3.0 M) and cleaned with the detergent (Hellmanex), water, acetone, and isopropanol subsequently. On top of the cleaned substrates, a 30-nm think of compact TiO_2 layer as electron transporting layer was spray-deposited from the titanium diisopropoxide bis(acetylacetonate) solution (Sigma-Aldrich) precursor diluted in isopropanol (1:15 by volume fraction) at 450 °C, followed by the deposition of a 100 nm thick mesoporous TiO_2 layer by spin-coating a diluted TiO_2 paste solution in ethanol (1:8 w/v) at 5000 rpm for 20 s and sintering at 500°C for 20 min. A 20 nm of tin oxide layer as a passivation layer was formed from the aqueous tin (IV) chloride solution (12 μL $SnCl_4$ for 1mL solution) by depositing the $SnCl_4$ precursor at 3000 rpm for 30 s, followed by annealing at

100°C for 10 min and 190°C for 60 min. UV-ozone treatment was carried out for 15 min before both SnO_2 layer deposition and perovskite layer deposition. A triple-cation based 3D perovskite precursor solution (1.3 M) with the composition of $[(FAPbI_3)_{0.87}(MAPbBr_3)_{0.13}]_{0.92}(CsPbI_3)_{0.08}$ was prepared by mixing the starting materials (FAI (GreatCellSolar), MABr (GreatCellSolar), CsI (ABCR), PbI_2 (TCI), and $PbBr_2$ (TCI)) in DMF and DMSO mixture with the volume ratio of 0.78:0.22. An excess of PbI_2 by 5% towards FAI was used in the precursor solution in order to control the growth of the 2D perovskite layer. The 3D perovskite layer was deposited by spin-coating the precursor solution at 2000 rpm for 12 s and 5000 rpm for 30 s. Chlorobenzene was poured on top of the spinning substrate 15 s prior to the end of the spin-coating process. The deposited 3D perovskite film was annealed at 100°C for 60 min. Then, the film was allowed to cool down to the room temperature and the corresponding thiophene methylammonium halide cations (60 mM in isopropanol) was deposited dynamically under 4000 rpm for 30 s. The film was then annealed at 100°C for 6 min on a hotplate. Spiro-OMeTAD (Merck) with a concentration of 60 mmol in 1 mL of chlorobenzene as hole-transporting material doped with 31.28 µL of 4-tert-butylpyridine (Sigma-Aldrich), 18.57 µL of Li-bis (trifluoromethanesulphonyl) imide (Aldrich) from the stock solution (196 mg in 379 µL acetonitrile), and 13.69 µL of FK 209 Co(III) TFSI (GreatCellSolar) from the stock solution (99 mg in 263 µL acetonitrile) was deposited by spin-coating at 4000 rpm for 30 s. Finally, a gold counter electode (70 nm) was deposited by physical vapor deposition process under high vacuum.

Thin-films Characterizations

Photoluminescence

Steady-state photoluminescence spectra were recorded on a Fluorolog3-22 spectrofluorometer upon excitation at 450 nm. The emission was measured from both top and bottom surface of the film.

UV-Vis absorption

An ultraviolet, visible, near-infrared spectrophotometer (PerkinElmer Lambda 950s) was used to measure the absorption spectra of the perovskite thin-films.

X-ray diffraction (XRD)

XRD patterns were acquired by measuring the perovskite thin-films using Bruker D8 Advance diffractometer and non-monochromated Cu-radiation. For the 2D/3D perovskite thin films, measurements under grazing incident diffraction (GID) geometry were performed on Bruker D8 Discover diffractometer with non-monochromated Cu-radiation at the incident angle of 2° in order to obtain the XRD patterns on the surface of the films.

Scanning electron microscopy (SEM)

SEM micrographs (cross-section and surface) were recorded in the FEI Teneo scaning electron microscope using in-lens detector under the accelerating voltage of 3 kV and 5 kV.

Ultra-violet photoemission spectroscopy (UPS) depth profiling (DP)

The samples were transferred to an ultrahigh vacuum chamber (ESCALAB 250Xi), with a base pressure of $2*10^{-10}$ mbar, for UPS DP measurements. UPS measurements were performed using a double-differentially pumped He gas discharge lamp emitting He I radiation (hν=21.22 eV) with a pass energy of 2 eV and a bias of -5 V in order to ensure secondary electron onset detection. The UPS spectra are shown as a function of the binding energy with respect to the Fermi Energy. The energy edge of the valence band features is used to determine the valence band level position with respect to the Fermi level and the secondary electron onset with combination of the latter are used to determine the vacuum level with respect to the Fermi level. The conduction bands were estimated using the optical gaps of the 2D and 3D materials. Cluster etching was performed using large Ar clusters generated by the MAGCIS Dual Beam Ion Source (Thermo Scientific) with an energy of 4000 eV.

Absolute Photoluminescence

Excitation for the PL measurements was performed with a 445 nm continuous wave laser (Insaneware) through an optical fibre into an integrating sphere. The intensity of the laser was adjusted to a 1 sun

equivalent intensity by illuminating a 1 cm2 size perovskite solar cell under short-circuit and matching the current density to the J SC under the sun simulator (22.0 mA cm–2 at 100 mW cm–2, or 1.375 × 1021 photons m–2 s–1). A second optical fiber was used from the output of the integrating sphere to an Andor SR393i-B spectrometer equipped with a silicon charge-coupled device camera (DU420A-BR-DD, iDus). The system was calibrated by using a calibrated halogen lamp with specified spectral irradiance, which was shone into to integrating sphere. A spectral correction factor was established to match the spectral output of the detector to the calibrated spectral irradiance of the lamp. The spectral photon density was obtained from the corrected detector signal (spectral irradiance) by division through the photon energy (hf) and the photon numbers of the excitation and emission obtained from numerical integration using Matlab. In a last step, three fluorescent test samples with high specified PLQY (≈70%) supplied from Hamamatsu Photonics were measured where the specified value could be accurately reproduced within a small relative error of less than 5%

All PL measurements were performed on complete cells, prepared fresh, and immediately encapsulated in a glovebox under N2 atmosphere. The PL of the samples was readily recorded after mounting the sample and after an exposure of 1 s at each laser intensity subsequently, the incident laser was blocked by a shutter and the filter wheel position adjusted while the sample was kept in dark conditions avoiding any effects induced by constant illumination. The cell was illuminated through the glass/ITO side. It was noted that all absolute PL measurements were performed on films with the same HTL, ETL, and perovskite thicknesses as used in the operational solar cells.

Photovoltaic characterization

The current density–voltage (J–V) curves were measured under 1 sun illumination (AM 1.5G) in the ambient atmosphere and temperature using xenon lamp solar simulator (450 W, Oriel, AAA class). The light intensity was calibrated to 1 sun by using a Si reference equipped with an IR-cutoff (KG5) filter (Oriel 91150V). The current responses were measured using a digital source meter (Keithley 2400) by applying an external voltage bias. A metal mask with aperture of 0.16 cm^2 was used during the measurement in order

to determine the active area. The J-V curves were scanned with the rate of 50 mV/s. No pre-biasing was applied prior to the measurements. External quantum efficiency (EQE) measurement was carried out by using IQE200B (Oriel).

Tables

Table 1 Photovoltaic parameters of the champion PSCs based on 3D perovskite and 2D/3D perovskite hybrids employing 2-TMAI, 2-TMABr and 2-TMACl tested under AM 1.5G illumination (100 mW cm^{-2}).

	V_{OC} (V)	J_{SC} (mA cm^{-2})	FF	PCE (%)
2-TMAI/3D	1.085	24.16	0.760	19.92
2-TMABr/3D	1.154	23.20	0.778	20.82
2-TMACl/3D	1.164	22.84	0.741	19.70
Control	1.087	24.19	0.787	20.68

References

1 Shao, S. & Loi, M. A. The Role of the Interfaces in Perovskite Solar Cells. *Advanced Materials Interfaces* **7**, 1901469 (2020).

2 Stolterfoht, M. *et al.* How To Quantify the Efficiency Potential of Neat Perovskite Films: Perovskite Semiconductors with an Implied Efficiency Exceeding 28%. *Adv. Mater.* **32**, 2000080 (2020).

3 Grancini, G. *et al.* One-Year Stable Perovskite Solar Cells by 2D/3D Interface Engineering. *Nat. Commun.* **8**, 15684 (2017).

4 Cho, K. T. *et al.* Selective Growth of Layered Perovskites for Stable and Efficient Photovoltaics. *Energy Environ. Sci.* **11**, 952-959 (2018).

5 Cho, K. T. *et al.* Water-Repellent Low-Dimensional Fluorous Perovskite as Interfacial Coating for 20% Efficient Solar Cells. *Nano Lett.* **18**, 5467-5474 (2018).

6 García-Benito, I. *et al.* Fashioning Fluorous Organic Spacers for Tunable and Stable Layered Hybrid Perovskites. *Chem. Mater.* **30**, 8211-8220 (2018).

7 Kim, H. *et al.* Optimal Interfacial Engineering with Different Length of Alkylammonium Halide for Efficient and Stable Perovskite Solar Cells. *Adv. Energy Mater.* **9**, 1902740 (2019).

8 Yoo, J. J. *et al.* An interface stabilized perovskite solar cell with high stabilized efficiency and low voltage loss. *Energy Environ. Sci.* **12**, 2192-2199 (2019).

9 Sutanto, A. A. *et al.* Dynamical evolution of the 2D/3D interface: a hidden driver behind perovskite solar cell instability. *J. Mater. Chem. A* **8**, 2343-2348 (2020).

10 Liu, Y. *et al.* Ultrahydrophobic 3D/2D fluoroarene bilayer-based water-resistant perovskite solar cells with efficiencies exceeding 22%. *Science Advances* **5**, eaaw2543 (2019).

11 Jung, E. H. *et al.* Efficient, Stable and Scalable Perovskite Solar Cells using Poly(3-hexylthiophene). *Nature* **567**, 511-515 (2019).

12 Bouduban, M. E. F. *et al.* Crystal Orientation Drives the Interface Physics at Two/Three-Dimensional Hybrid Perovskites. *J. Phys. Chem. Lett.* **10**, 5713-5720 (2019).

13 Kim, J., Ho-Baillie, A. & Huang, S. Review of Novel Passivation Techniques for Efficient and Stable Perovskite Solar Cells. *Solar RRL* **3**, 1800302 (2019).

14 Ng, C. H. *et al.* Reducing trap density and carrier concentration by a Ge additive for an efficient quasi 2D/3D perovskite solar cell. *J. Mater. Chem. A* **8**, 2962-2968 (2020).

15 Zuo, C. *et al.* Crystallisation control of drop-cast quasi-2D/3D perovskite layers for efficient solar cells. *Communications Materials* **1**, 33 (2020).

16 Luo, D., Su, R., Zhang, W., Gong, Q. & Zhu, R. Minimizing non-radiative recombination losses in perovskite solar cells. *Nat. Rev. Mater.* **5**, 44-60 (2020).

17 Braly, I. L. *et al.* Hybrid perovskite films approaching the radiative limit with over 90% photoluminescence quantum efficiency. *Nat. Photon.* **12**, 355-361 (2018).

18 Liu, Z. *et al.* Open-Circuit Voltages Exceeding 1.26 V in Planar Methylammonium Lead Iodide Perovskite Solar Cells. *ACS Energy Lett.* **4**, 110-117 (2019).

19 Sutanto, A. A. *et al.* In Situ Analysis Reveals the Role of 2D Perovskite in Preventing Thermal-Induced Degradation in 2D/3D Perovskite Interfaces. *Nano Lett.* **20**, 3992-3998 (2020).

20 Lami, V. *et al.* Visualizing the Vertical Energetic Landscape in Organic Photovoltaics. *Joule* **3**, 2513-2534 (2019).

21 Lami, V., Hofstetter, Y. J., Butscher, J. F. & Vaynzof, Y. Energy Level Alignment in Ternary Organic Solar Cells. *Advanced Electronic Materials* **n/a**, 2000213.

22 Zhang, J. *et al.* Sequentially Deposited versus Conventional Nonfullerene Organic Solar Cells: Interfacial Trap States, Vertical Stratification, and Exciton Dissociation. *Adv. Energy Mater.* **9**, 1902145 (2019).

23 Wittmann, A. *et al.* Tuning Spin Current Injection at Ferromagnet-Nonmagnet Interfaces by Molecular Design. *Phys. Rev. Lett.* **124**, 027204 (2020).

24 Fassl, P. *et al.* Fractional deviations in precursor stoichiometry dictate the properties, performance and stability of perovskite photovoltaic devices. *Energy Environ. Sci.* **11**, 3380-3391 (2018).

25 Cui, P. *et al.* Planar p–n homojunction perovskite solar cells with efficiency exceeding 21.3%. *Nat. Energy.* **4**, 150-159 (2019).

26 Diekmann, J. *et al.* Pathways towards 30% efficient perovskite solar cells. Preprint at https://arxiv.org/abs/1910.07422 (2019).

27 Caprioglio, P. *et al.* On the Origin of the Ideality Factor in Perovskite Solar Cells. *Adv. Energy Mater.* **10**, 2000502 (2020).

28 Stolterfoht, M. *et al.* The impact of energy alignment and interfacial recombination on the internal and external open-circuit voltage of perovskite solar cells. *Energy Environ. Sci.* **12**, 2778-2788 (2019).

29 Caprioglio, P. *et al.* On the Relation between the Open-Circuit Voltage and Quasi-Fermi Level Splitting in Efficient Perovskite Solar Cells. *Adv. Energy Mater.* **9**, 1901631 (2019).

30 Stolterfoht, M. *et al.* Voltage-Dependent Photoluminescence and How It Correlates with the Fill Factor and Open-Circuit Voltage in Perovskite Solar Cells. *ACS Energy Lett.* **4**, 2887-2892 (2019).

31 Stolterfoht, M. *et al.* Visualization and suppression of interfacial recombination for high-efficiency large-area pin perovskite solar cells. *Nat. Energy.* **3**, 847-854 (2018).

32 Wolff, C. M., Caprioglio, P., Stolterfoht, M. & Neher, D. Nonradiative Recombination in Perovskite Solar Cells: The Role of Interfaces. *Adv. Mater.* **31**, 1902762 (2019).

33 Wang, Q. *et al.* Large Conduction Band Energy Offset Is Critical for High Fill Factors in Inorganic Perovskite Solar Cells. *ACS Energy Lett.* **5**, 2343-2348 (2020).

Acknowledgements

We acknowledge Dr. Pascal A. Schouwink for the assistance in grazing-incident angle XRD measurements. We acknowledge the Swiss National Science Foundation (SNSF) funding through Synergia Grant

EPISODE (Grant No. CRSII5_171000). This project has received funding from the European Research Council (ERC) under the European Union's Horizon 2020 research and innovation programme (ERC Grant Agreement n° 714067, ENERGYMAPS) and the Deutsche Forschungsgemeinschaft (DFG) within the framework of SPP 2196, project PERFECTPVs (project #424216076). G.G. acknowledges the "HY-NANO" project that has received funding from the European Research Council (ERC) Starting Grant 2018 under the European Union's Horizon 2020 research and innovation programme (Grant agreement No. 802862). MS acknowledges the DFG - project number 423749265 and 03EE1017C - SPP 2196 (SURPRISE and HIPSTER) for funding. The authors acknowledge the Swiss National Science Foundation (SNSF) funding through the Ambizione Energy project Hyper (Grand number PZENP2_173641).

Author contributions

G.G., A.A.S., and D.N. conceived the original idea of the work. N.D. designed the organic salts, A.A.S. fabricated the thin films and PSCs and characterised them, I.G.B. performed the initial 2D materials investigation and V.I.E.Q. performed the steady-state PL measurements, with and under the supervision of G.G.

P.C. and M.S. performed the PLQE measurement, QFLS calculation, and drift-diffusion simulation.

Y.J.H. performed the UPS depth profiling measurements and analysis together with and under the supervision of Y.V.

G.G., A.A.S., P.C., M.S. and Y.V. designed the experiments, analyzed the results and discussed the main conclusions of the work.

M.K.N., D. N., M. S., Y.V. and G. G. supported and supervised the project. A.A.S., P.C., M.S., Y.V., and G.G. wrote the manuscript, which was edited by all the authors.

Competing interests

The authors declare no competing interests.

Figures

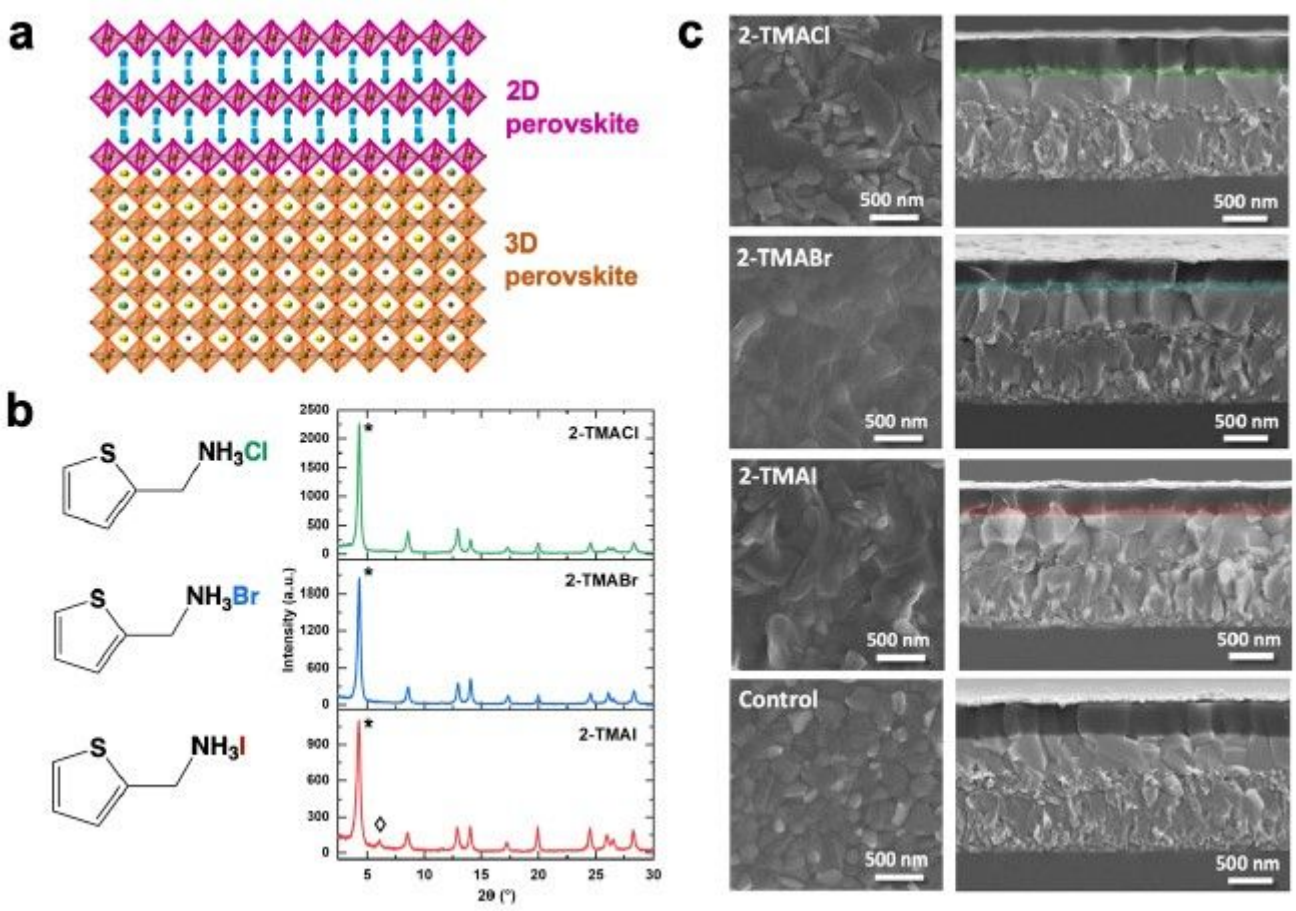

Figure 1

Structural and morphological characterization of 2D/3D perovskite films. a Schematic illustration of the 2D/3D perovskite interface. b Molecular structure (left) and X-ray diffraction (XRD) pattern at 2° incident angle of the 2D/3D film employing 2-TMAI, 2-TMABr, and 2-TMACl respectively (* and ◊ denote 2D perovskite phase with n=1 and n=2, respectively). c Top view (left) and cross-section (right) micrographs of the 3D only device as control and the 2D/3D perovskite solar cells (PSCs) employing 2- TMAI, 2-TMABr, and 2-TMACl.

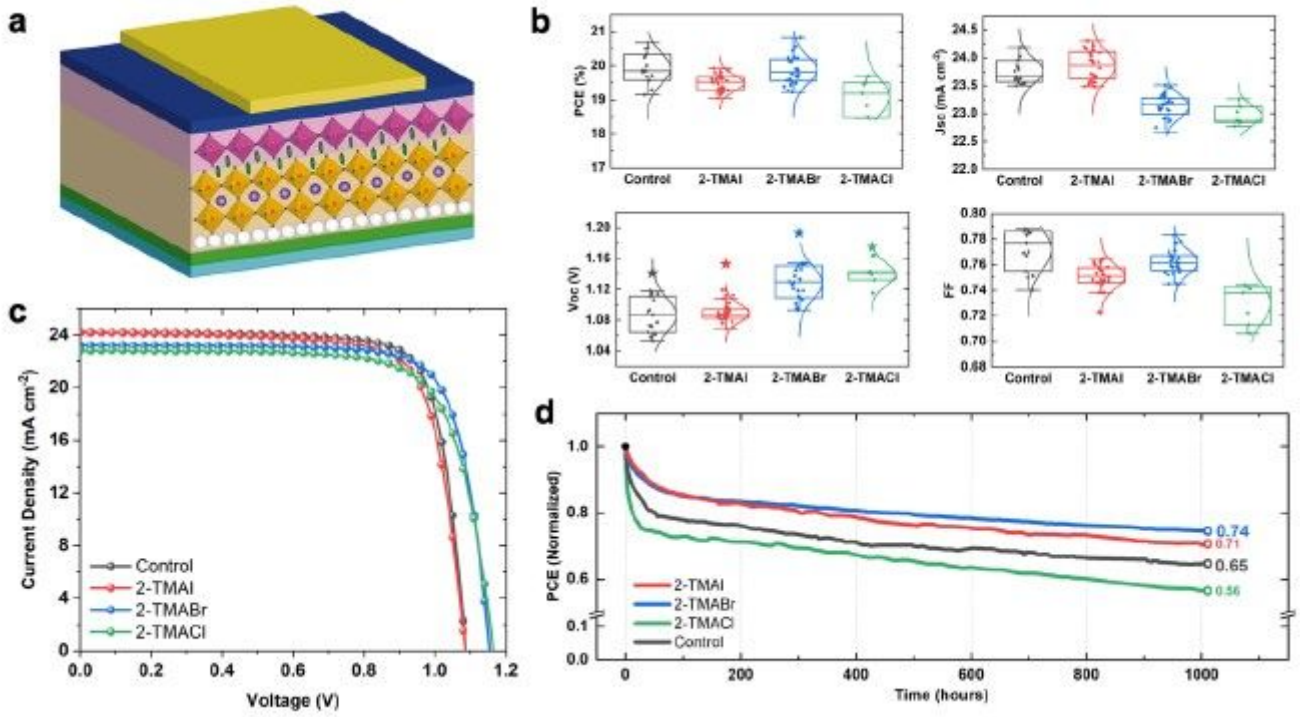

Figure 2

Photovoltaic performances of 2D/3D perovskite solar cells (PSCs). a Schematic device structure of the 2D/3D PSCs. b Statistics of the photovoltaics parameters of 3D PSCs as a control and 2D/3D PSCs based on 2-TMAI, 2-TMABr, 2-TMACl on over 70 devices. Note that the stars symbols in the VOC subpanel represent the VOC measured without using a mask. c J-V curves of the champion cells of 3D and 2D/3D PSCs employing 2-TMAI, 2-TMABr, and 2-TMACl. d Stability test under continuous 1 sun illumination for 1000 h in inert gas (Ar) atmosphere without any encapsulation.

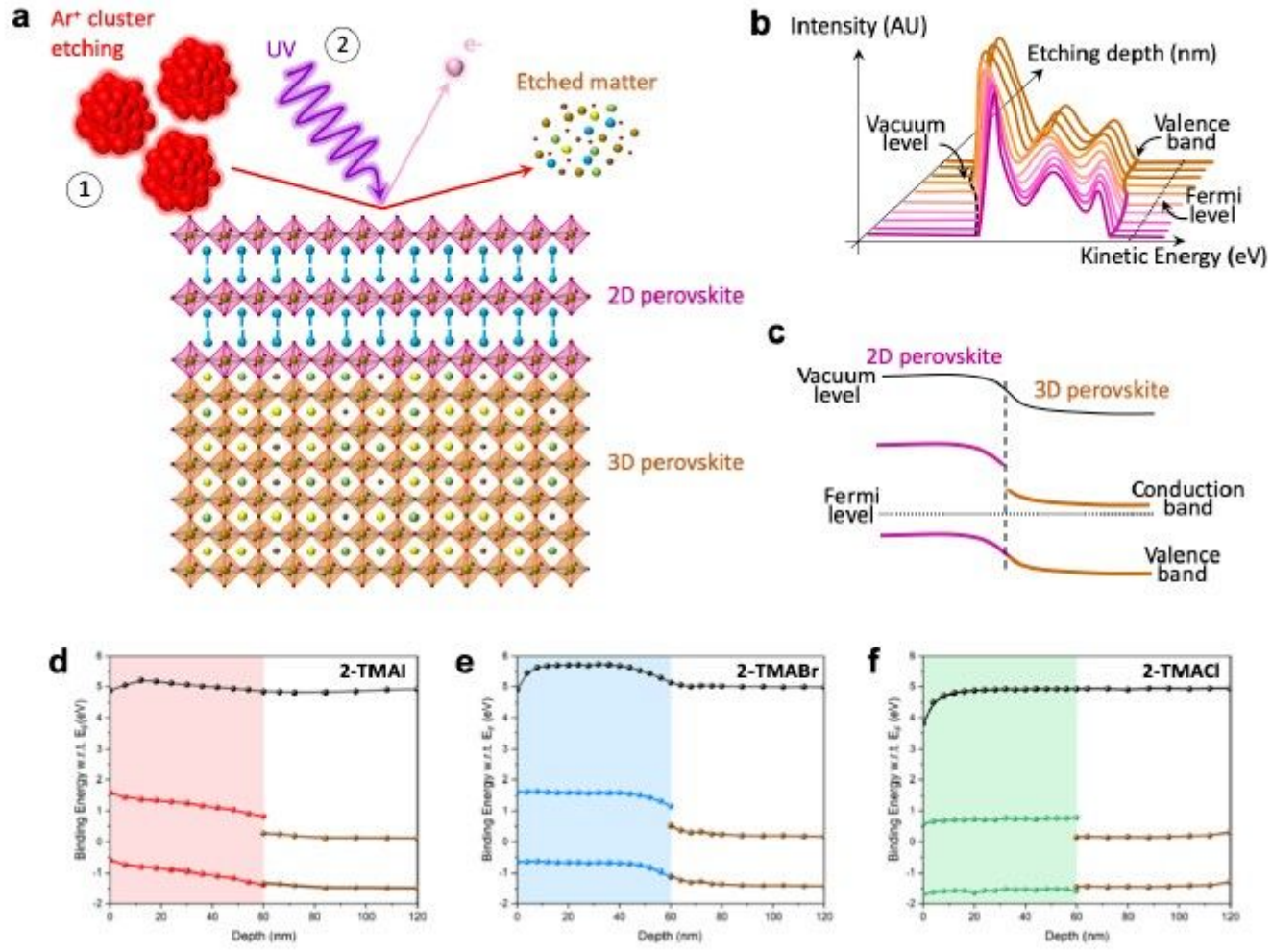

Figure 3

UPS depth measurement of 2D/3D perovskite interface. a Schematic representation of the UPS depth profiling technique which combines (1) etching by Ar ion clusters with (2) UPS measurements. b,c illustration of the evolution of the UPS spectra as a function of depth (b) and the corresponding energy level diagram extracted from b (c). d-f Measured energetic level diagrams of 2-TMAI (d), 2-TMABr (e), and 2-TMACl (f) with the 3D perovskite layer.

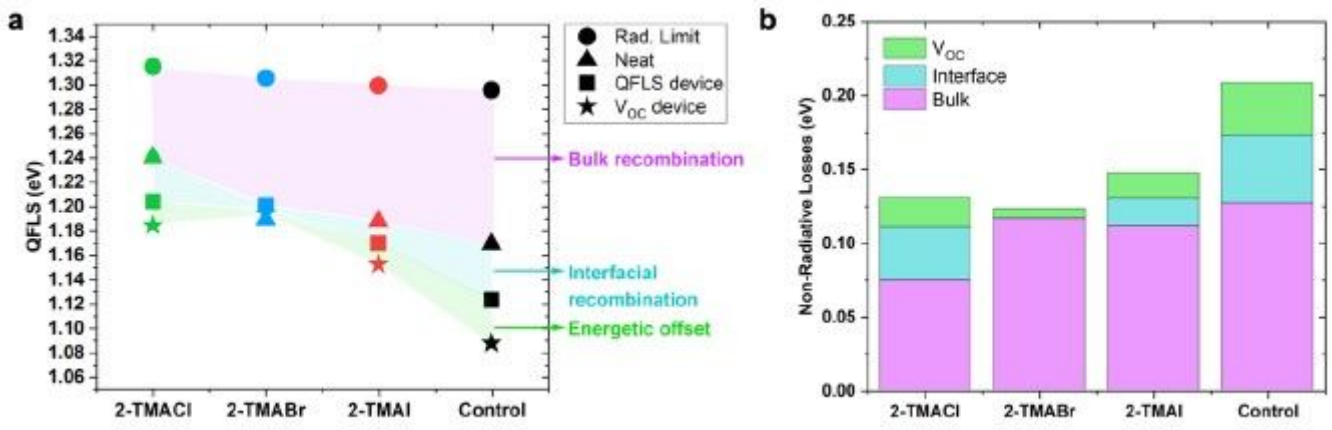

Figure 4

Calculated QFLS and calculated energy losses due to non-radiative recombination. a QFLS calculated from PLQY for the neat material and the full device for the different samples investigated in the study. Here the Shockley-Queisser radiative limit and the experimental VOC of each sample are plotted. b Different type of energy losses calculated from a in order to compare the contribution of the different recombination processes for each system.

Supplementary Files

This is a list of supplementary files associated with this preprint. Click to download.

- SutantoetalSI.pdf
- FigureS1.jpg
- FigureS2.jpg
- FigureS3.jpg
- FigureS4.jpg
- FigureS5.jpg
- FigureS6.jpg
- FigureS7.jpg
- FigureS8.jpg
- FigureS9.jpg
- TableS1.png
- TableS2.png